national accelerator laboratory

FN-234
2526.000

A NOVEL MASS-SENSITIVE IMAGE-DISSECTING CERENKOV DETECTOR*

Arthur Roberts

July 27, 1971

ABSTRACT

This note describes a Cerenkov detector system specifically designed to provide an independent identifying trigger signal for each of the different particles present in the NAL 150 GeV/c charged hyperon beam. The detector must be used in conjunction with a magnetic channel and a quadrupole focusing lens pair (or triplet). The expected detection efficiency for particles within its 140-160 GeV/c momentum acceptance band is over 90% for all particles lighter than the deuteron; for anti-deuterons it exceeds 80%. Electrons, muons, pions and kaons are not distinguished from each other in the present design. All other known particles up to and including the deuteron mass are distinguished from each other and from the light particles. Specific triggers are provided for $(e\mu\pi K)^-$, $\bar{p}$, Σ^-, Ξ^-, Ω^-, and anti-deuterons. For each of these particles, separate triggers are available for at least three momentum ranges within the acceptance band. Rejection ratios for unwanted particles are expected to exceed 10^3.

*Submitted to Rochester Meeting of DPF, August-September 1971.

FN-234
2526.000

I. INTRODUCTION: PARTICLE BEAM

For experiments on hyperon interactions and decays it is highly desirable to have available a prompt signal that unequivocally identifies the beam particle and can be incorporated into a trigger logic. Differential Cerenkov counters appear to be suited to this purpose, since they are readily capable of the necessary resolution, even without correcting for chromatic dispersion. However, differential Cerenkov counters normally detect only one kind of particle at a time, and require a highly collimated beam[1]. Previous attempts[2] at Cerenkov detectors for the NAL 150 GeV/c hyperon beam have been seriously compromised in efficiency because the beam, as originally designed without quadrupole focusing, is too diffuse. It contains particles from 130 to 170 GeV/c, has a horizontal spread of about 1.0 cm, an angular dispersion of 0.125 mrad/GeV/c, and an angular spread of about 1.0 mrad at any given momentum. The vertical phase space is 1.0 cm by 1.9 mrad. The only known Cerenkov detector capable of dealing with such a beam is the cascaded image-intensifier ring detector first proposed by the author[3], which does not deliver a prompt signal.

The addition of quadrupole focusing to the beam greatly simplifies the Cerenkov detector design. The increased length of beam due to the quadrupoles (3.5 meters) results in some particle loss by decay; the sigma and xi decay lengths at 150 GeV/c are both 5.6 meters. The loss is more than compensated, however, by the increased detection and triggering efficiency that becomes possible. Furthermore, the beam

characteristics have made possible the design of a novel adaptation of the ring-image detection system, using photo-multiplier detectors, that meets all the objections raised above, and yields with high efficiency individual triggers for each type of particle in the beam. The counter design is inseparably bound to that of the beam, since only very carefully controlled beam optics permit the separation required.

Figure 1 shows a drawing of the hyperon beam. The secondary (diffracted) proton beam, of nominal energy 200 GeV/c or less, strikes a small target T, of cross-section 1 mm square. The hyperons are selected by a small channel in a five-meter long magnet, which is also part of the hadron shield for the target. The magnet is especially designed to avoid focusing unwanted muons into the beam channel; for this purpose the gap is wide and the coils remote for the channel[4]. The channel is 3 mm wide at the entrance, 10 mm at the exit, and its height is 10 mm. The nominal magnetic field is 30 kilogauss, which gives 30 mrad deflection at 150 GeV/c. The momentum dispersion in the channel is consequently quite small, and the emerging beam has the unpleasant characteristics enumerated above. The momentum spread is so wide that fast xi's, for example, have a higher velocity than the slowest sigmas, so that separation by volocity alone is not possible.

II. ADDITION OF QUADRUPOLE LENSES

The addition of a double-focusing quadrupole pair, designed to focus from point source (at the target), to

parallel, produces a vastly improved beam. The bending dipole has little effect on the focusing, since its field is strictly uniform and end effects are almost negligible. It does, however, provide momentum dispersion. The characteristics of the resulting beam are shown in Figures 2-5. These figures represent the phase space occupied by the beam at the quadrupole exit. Figure 2 shows the horizontal spread of the beam as a function of momentum. The momentum dispersion is represented by the change of position with momentum of the center of gravity of the distribution at any given momentum. The total horizontal spread for the momentum range 140-160 GeV/c is about 1.6 cm. At any given horizontal position the momentum spread is about 15 GeV/c.

Figure 3 shows the angle or direction in the horizontal plane as a function of momentum. We note that the angular dispersion of the beam is 0.15 mrad/GeV/c, and that the angular spread at a given momentum is only $\pm$ 0.1 mrad or so. This means that measuring the direction of a particle can give its momentum to within about 1 GeV/c.

Similarly, in the vertical direction, Figure 4 shows that particles of all momenta are uniformly spread over about 2.4 cm. However, Figure 5 indicates that the beam has remarkable parallelism: the spread ranges from $\pm$ 0.04 mrad at the waist (which comes at 159 GeV/c, indicating a need for retuning) to $\pm$ 0.10 mrad at a point $\pm$ 10 GeV/c away. The vertical angular divergence is actually less

than that due to chromatic dispersion in the Cerenkov medium at the angles used.

We thus have a beam which is essentially parallel in the vertical dimension, and in which the horizontal direction of the particles is determined by its momentum; such a beam is almost ideally suited to Cerenkov analysis. The vertical parallelism means that the axes of the Cerenkov light cones (that is, the particle trajectories) are all parallel to or lie in one plane. Therefore, the centers of the ring images formed by a spherical mirror from these cones will lie on a straight horizontal line. The centers of the ring images for all particles of a given momentum will essentially coincide, since the momentum corresponds closely to direction. Now the identification of a particle and the measurement of its momentum require the determination of a) the location of the center of the ring image, and b) its radius. The fact that the centers lie on a straight line and are uniformly dispersed along it, according to momentum, greatly simplifies the task.

III. IMAGE GEOMETRY

Figure 6 shows an example of the ring images to be expected. The common centers of rings corresponding to momenta of 140, 150 and 160 GeV/c are indicated. A series of rings representing the images produced by antideuterons, omega-minus, and xi hyperons are shown, one for each particle at each of these three momenta. The radius of each ring is proportional to the cone angle. The very wide separation of these particles is due to the fact that they are relatively

near threshold for the index of refraction chosen (n = 1.00011). However, one important and unexpected fact is observed: for each particle there is an approximate geometrical focusing of the circles to a common focal spot in the second quadrant (and its mirror image in the fourth). Light falling in this area is uniquely due to one kind of particle. The resolution shown here is relatively good because of the masses selected. Figure 7 shows the ring images for all the particles expected, including not only the three shown in Figure 6 but also the sigma, antiproton, kaon and pion. There exists an approximate focus for each particle, which approaches the 90° position as the velocity approaches unity.

Given enough light, a slit at each such focus would suffice to select each kind of particle uniquely. However, the constants chosen for the Cerenkov radiator (n = 1.00011, length 5 meters) represent a compromise between good resolution (which requires small cone angles) and good light output, which requires large angles. With the constants chosen, we expect about 10 photoelectrons for a pion, ranging down to about 5 for an omega and only 2 for the lowest momentum antideuteron. Thus a small fraction of the ring circumference is insufficient to give high counting efficiency. Increasing the cone angle not only decreases the angular separation, but makes the chromatic dispersion relatively larger. Consequently our detection must use a larger fraction of the ring image.

Furthermore, if we select only the region of the focus for each particle, we reject useful information. The available data determine the particle mass even in the absence of

a focus, over a wide range of mass values. To see this we note that to determine the mass, we need both velocity and momentum. Locating the center of the circle will determine the direction, and hence the momentum; the velocity is given by the radius. Locating the points of intersection of the circle with the momentum-dispersing axis yields both these quantities; thus a series of narrow slits perpendicular to the axis would serve to identify masses. In practice, we divide the whole area up into approximately circular zone-segments, taking due account of the actual geometry of the ring images as given by Figure 7. Each segment carries information, and identification is obtained by judicious combination. Examples are given below. Cerenkov detectors using similar geometries and coincidence systems have been successfully used at light levels similar to those contemplated here.[1,6]

IV. LIGHT COLLECTION

The problem of collecting the light from various segments of the image plane area seems to be best solved by the use of an array of concave mirror segments as slits. Each segment can focus the light incident upon it to a spot in the focal plane of the mirror of which it is a segment. If the incident light were parallel and aberrations were absent, the image thus formed would be a point. The slightly converging light from the Cerenkov reflector will again diverge after reflection at the image plane giving a bundle of rays whose finite size determines the minimum aperture required of the photomultiplier detector. This turns out

to be considerably less than the size of photomultiplier selected on grounds of economy (1.5" diameter). The bilateral symmetry of the ring images, above and below the momentum dispersion axis (see Figure 6) allows the use of one photomultiplier for each pair of symmetrical mirror segments.

The phototubes cannot be axially located without intercepting the incident Cerenkov radiation; so they must be located outside the cone of incident light. This requires the mirror segments to be tilted outward to steer the corresponding images onto the appropriate phototubes. Figure 8 illustrates how a pair of mirror segments can be arranged to reflect the incident Cerenkov light to a photomultiplier. 8a shows the two mirror segments, symmetrically opposite each other; 8b shows how the light is imaged off-axis to a single photomultiplier which lies in the plane of the segment mirror axis and the axis of the Cerenkov reflector.

V. MIRROR GEOMETRIES

The division of the focal plane into mirror segments is governed by the obvious considerations: separation of all the various masses, momentum range covered and detection efficiency. These must be balanced against the complexity which inevitably accompanies higher performance standards.

A true optimization of the design may well be a long and time-consuming process and has not been attempted. In the course of evaluating and proving basic concepts, we have arrived at what appears to be a satisfactory and practical design, which will now be described. It uses the magnetic

channel and quadrupole pair described above in Section I, and the Cerenkov detector parameters of Table 1. Figure 9 shows an overall layout of the Cerenkov detector, and Figure 10 a drawing of the focal plane mirror segmentation. Figure 11 shows the array of photomultipliers that detect the light reflected from the mirrors of Figure 10. Once the location and focal length of these mirror segments has been determined, the details of construction of the mirrors can be decided. From Figure 8 one can see how to select, for each segment and its corresponding photomultiplier location, what portion of the mirror to cut out, and what the angles of tilt with the optical axis must be.

VI. LOGICAL SELECTION

A comparison of Figure 10, the mirror segmentation, with Figure 7, the trajectories of the ring images, will indicate how the distinction among the various particle masses can be made (an overlay would show it better). By tracing out each trajectory a list of the segments intersected and the arc length in each can be made. Some, including those containing the trajectory "focus", are intersected by only one kind of particle. They are Nos. 1, 6, 7, 8, 12, 13, 14 and 28. Others are seen by two, three, or four different particles; and a suitable logical connection of the photomultiplier outputs is required in order to yield both complete purity of selection as well as high detection efficiency.

We now describe the logic used in our demonstration system. The calculations have been made by hand, not by computer; consequently we have not been able to sample all momentum

values in the 140-160 GeV/c range. Rather we have studied the trajectories at three momenta: 140, 150 and 160 GeV/c, and examined their behavior as the momentum changes, particularly as they cross the boundaries of mirror segments. Table 2 shows a truth table for the mirror configuration, i.e., the mirrors intersected by each particle at each of the three momenta selected. By pions we understand all lighter particles as well; and although we separately list pion and kaon, no attempt has been made in the logic to separate them, since in the contemplated use these are both background particles. (Separation is perfectly feasible, however, at a somewhat lower index of refraction, with a different mirror arrangement.)

A sample of the logical selection is shown in Table 3 which shows the coincidence requirements used to identify each momentum for sigma and xi. Not all logically possible combinations are necessary; the detection efficiency determines how many are needed. Coincidences of order higher than twofold have not in general been used (one exception is $\Xi(160)$); they are necessary only if the detection efficiency is otherwise too low. The complete logic table is contained implicitly in Figure 12, which shows the matrix of photomultiplier outputs used to obtain the appropriate twofold trigger outputs. The only additional logical elements required are appropriate "or" circuits to combine the outputs into the desired triggers, which may be segregated by particle, or by both particle and momentum.

Chromatic Aberration. The Cerenkov rings are not of zero width, not only because of optical imperfections but because of the variation of the index of refraction n over the range of light wavelengths accepted. In fact, to restrict the chromatic dispersion and also to keep the cost of photomultipliers low, a cut-off in the ultraviolet at about 300 nm has been accepted; this keeps the angular width of the ring to about 2% if neon, which has low dispersion, is used. Momentum (or mass) resolution of the detector is limited by chromatic dispersion; in the contemplated use this limitation is without significance. The achromatization techniques of the DISC counters have not been investigated.

VII. DETECTION EFFICIENCY

The number of photoelectrons to be expected from a photocathode illuminated by light from a Cerenkov radiator is given by an expression of the form

$$N = N_o \cdot L \cdot \sin^2\theta$$

where L is the length of the radiator in cm, and N_o is a constant depending on the range of wavelengths accepted and the efficiency of the photocathode used; θ is the Cerenkov cone angle. For bialkali cathodes and quartz windows, values of N_o approaching 150 have been reported; in view of our cutoff at 300 nm a value of 100 is reasonable. We will later investigate the effects of varying N_o. It is, of course, essential in this type of detector that the phototubes used be capable of high efficiency when recording only a single photoelectron. This implies a low noise background. Bialkali cathodes are desirable in this respect too.

Figure 13 shows the number of photoelectrons to be expected in collecting all the light in a Cerenkov ring produced in a radiator 5 meters long, with N_o = 70 or 100 respectively. Table 4 shows the angular radius of the ring for the particles of interest to us. It will be seen that the largest number of photoelectrons is about 10, for pions, decreasing to two for the lowest momentum antideuterons, which are at the very threshold of detection with this value of n.

It is now readily possible to calculate the detection efficiency for any desired particle and momentum. The fraction of the total ring occupied by the image in each mirror segment is first found; from this the most probable number of photoelectrons in the corresponding phototube is found. If this number is p, the chance of getting a non-zero number of photoelectrons in that tube is 1 - exp (-p); this is the efficiency of the segment. From this the detection efficiency for each selection logic in the trigger system can be calculated, and combined to yield the probability of detection of each particle. Table 5 shows the most probable number of photoelectrons in the several segments, and the corresponding detection efficiencies, for sigma and xi hyperons. Using the logical selection of Table 3 we find the overall detection efficiency. Table 6 shows the calculated overall efficiency for all particles; it also shows the effect of reducing the constant N_o from 100 to 70, on the detection efficiency for xi's. The relatively small decrease in detection efficiency indicates, for all but the

heaviest particles, a heartening insensitivity to optical losses and cathode variability.

VIII. BACKGROUND REJECTION

An important characteristic of a mass-sensitive detector is its ability to reject spurious signals from particles of the wrong mass. In the present system the mass selection is performed almost entirely by twofold coincidences characteristic of the desired particle, and corresponds to the minimum logic necessary for identification. This is the arrangement giving highest detection efficiency. Background particles will in the majority of cases also produce triggers in one of the coincident pair; then any accident producing a count in the other will produce a spurious signal. Such accidents include tube noise, delta-rays, or decay in flight. Tube noise is minimized by using low-noise tubes, and can be eliminated by cooling the photocathodes, if necessary. The other signals are due to other particles.

Normally, spurious background is reduced by using higher order coincidences, which introduce logical redundancy; Meunier[7] recommends six or more. Such rejection diminishes detection efficiency. Curves illustrating the variation of background rejection and efficiency with coincidence multiplicity, for a differential Cerenkov counter, have been published by Denisov, et al.[1] Good rejection is readily attainable; each additional order of coincidence produces more than an order of magnitude drop in background.

Improved rejection can also be obtained by detecting the light falling outside the desired ring and using the signal so

produced in anticoincidence. Ozaki, Russell, Sacharidis and Reed[8] detected kaons with over 80% efficiency, with pion and proton rejection ratios over 10^5. This technique is available to us already, since we possess selection signals for each of the unwanted particles that can readily be used in anticoincidence. But it is possible to do still better. For each particle, all mirror signals not required to produce the trigger may be placed in anticoincidence. Thus, e.g. for Xi(140), which illuminates only segments 4, 10, 11, 17 and 21, all other mirrors can be in anticoincidence, yielding very high rejection ratios. For Σ (140) it may be verified from Table 5b that the anticoincidence efficiency is 99.92%. Consequently we anticipate attainable rejection ratios of 10^3 or better.

IX. CONSTRUCTION AND CALIBRATION

The most difficult technical aspect of construction appears to be the fabrication and assembly of the concave mirror segments in the ring image plane, shown in Figure 10. Having devoted considerable thought to this problem, we propose the following procedure. First, several spherical brass mirrors, about 8-10 inches in diameter, of 55 cm focal length, will be approximately machined on a template-following lathe, to an accuracy of the order 0.001". These mirrors will then be ground and polished. The pattern of segments to be cut will be laid out on the mirrors, and the segments will then be roughed out, using a small endmill.

The segment will then require only careful contouring to achieve the correct final shape. Finally the segments can

each be mounted on an adjustable ball joint, all of which are in turn mounted on a flat plate.

To align the mirrors, a ring of light of variable radius is needed; the center can be moved by moving either source or mirror plane. Narrow light rings can be made by producing Cerenkov-like cones from parallel light with a conical lens, or axicon. A spherical mirror will then convert such a cone to a ring image in the focal plane of the mirror. The radius of the ring is proportional to the cone angle, the location of its center determined by the direction of the cone axis. To vary the radius of the ring image one varies the light cone angle. This is most readily done with a hollow lucite axicon which can be filled with liquids of different indices of refraction. A mixture of water and glycerine covers the range $n = 1.33$ to 1.67. The half-angle of the light cone generated by an axicon of index n and half-angle $90° - \theta$ is $(n - 1)\theta$. Thus we can cover a factor of two in cone angle with a single axicon.

REFERENCES

[1]See, e.g. S. P. Denisov, S. V. Donskov, Yu. P. Gorin, R. N. Krasnokutsky, A. I. Petrukhin, Yu. D. Prokoshkin, R. S. Shuvalov and D. A. Stoyanova, Nuclear Instruments and Methods 92 (1971), 77.

[2]A. Roberts, M. Atac and R. Stefanski, Internal NAL Memo (unpublished), May 7, 1970; R. L. Sumner, T. M. Knasel, E. C. Swallow and R. Winston, Report EF 71-18, Enrico Fermi Institute, University of Chicago (April 1971) unpublished.

[3]A. Roberts, Rev. Sci. Instr. 31, 579 (1960); A. Roberts, Nuclear Instruments and Methods 9, (1960), p. 55.

[4]This magnet was designed by R. March.

[5]The quadrupole lens design was carried out by R. Stefanski, who also evaluated the beam phase space.

[6]S. P. Denisov, S. V. Donskov, A. F. Dunaitsev, Yu. P. Gorin, A. I. Petrukhin, Yu. D. Prokoshkin, R. S. Shuvalov, D. A. Stoyanova, Nucl. Instr. and Methods 85, (1970), 101.

[7]R. Meunier, NAL 1970 Summer Study, SS-170, p. 85. National Accelerator Laboratory, Batavia, Illinois.

[8]S. Ozaki, J. J. Russell, E. J. Sacharidis, and J. T. Reed, Nucl. Instr. and Methods 35, (1965), p. 301.

Table 1. Cerenkov Counter Constants.

Radiator length:	5.0 meters
Radiator gas:	Neon at about 1.65 atmospheres
Index of refraction:	1.00011
Maximum cone angle:	14.7 mrad
Momentum acceptance:	140-160 GeV/c
Cerenkov mirror diameter:	8 in.
Focal length:	5.5 - 6.0 m
Wavelength range used:	300 - 600 nm.
Phototubes:	Probably RCA 4517.

Table 2. Truth Table for mirror segments of Fig. 10 intersected by ring images of Fig. 7. Diagonal lines and arrows imdicate smooth transitions with varying momentum.

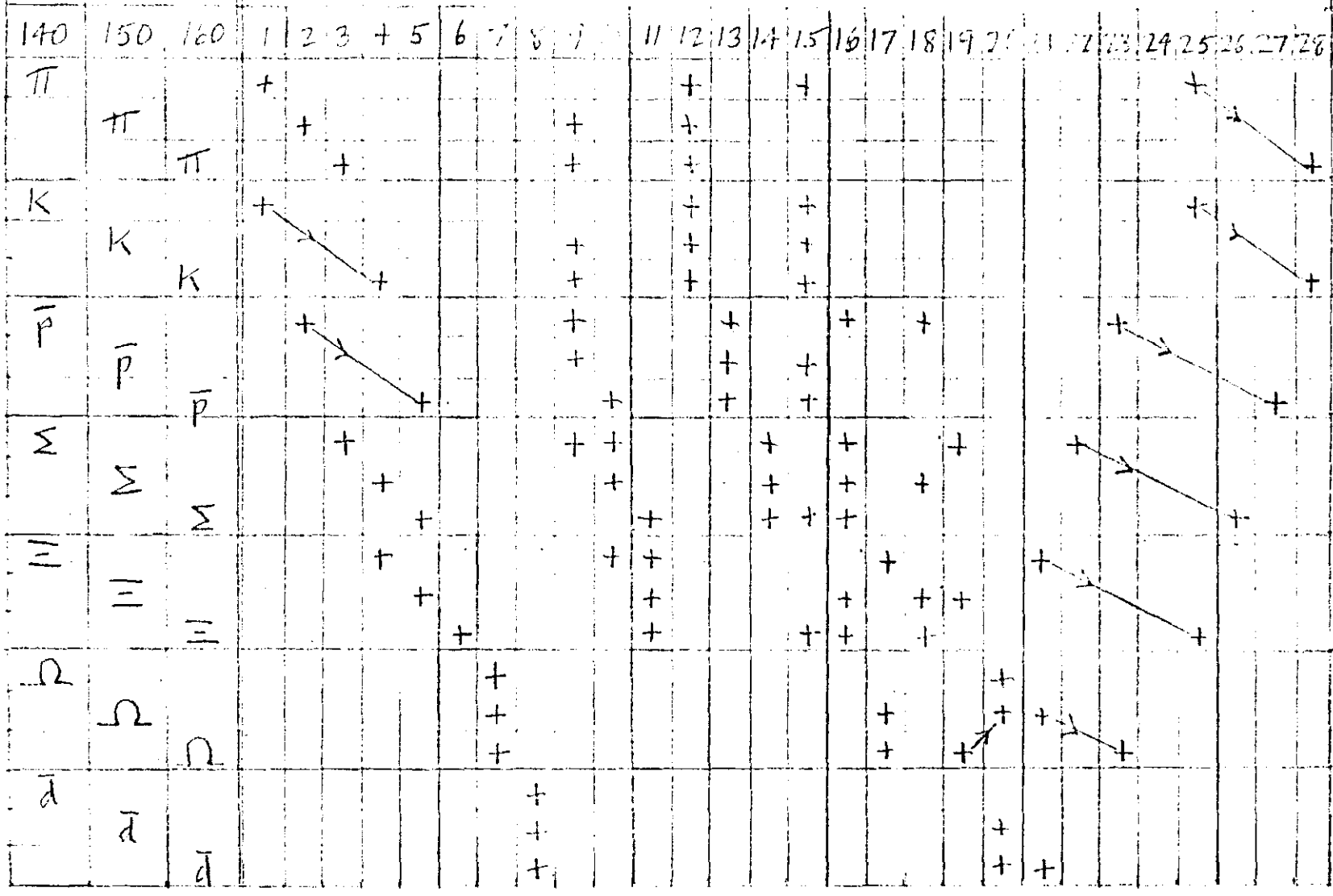

FN-234
2526.000

Table 3. Examples of logical selection: Sigma and Xi hyperons.

Note: Sigma trigger 14 does not distinguish sigma momentum; all others do.

Particle, Momentum	Logical Selection
Ξ, 140	4·(11 + 17 + 21) + 11·(10 + 17 + 21) + 10·21
Ξ, 150	(18 + 22)·(5 + 11 + 16) + 18·22
Ξ, 160	6 + (11 + 15)·(16 + 18 + 24) + 18· 24
Σ, 140	14 + 3·(10 + 19 + 22) + 9·(19 + 22) + 10 ·(9 + 16 + 22)
Σ, 150	14 + 24·(4 + 5) + 10·(16 + 18 + 24)
Σ, 160	14 + 5·26 + 16·(5 + 26) + 5·15·(11 + 16)

Table 4.

Angular radii for n = 1.00011 (in mrad)

Particle	Momentum, GeV/c		
	140	150	160
Pion	14.40	14.43	14.48
Antiproton	13.22	13.45	13.62
Sigma	12.12	12.51	12.81
Xi	11.45	11.96	12.33
Omega	8.79	9.78	10.52
Antideuteron	6.43	8.02	9.12

Table 5A. Most probable number of photoelectrons produced by light incident upon a mirror segment.

Particle, Momentum, Gev/c	SEGMENT NUMBER																					
	3	4	5	6	9	10	11	12	14	15	16	17	18	19	20	21	22	23	24	25	26	
Sigma 140	1.33				1.11	.90			.67		1.33			.9								
Sigma 150		1.33				1.80			.90		1.33		.9						1.8			
Sigma 160			2.2				.90		.90	1.33		.67									1.8	
Xi 140		1.16				.78	1.54					1.16				1.79						
Xi 150			1.54				1.36				1.16		.78	.19				1.55				
Xi 160				1.54			1.36			.39	1.16		.39							1.55		

Table 5B. Corresponding detection efficiency.

Sigma 140	.73				.67	.59			.49		.73			.59				.53				
Sigma 150		.73				.53			.59		.73		.59						.53			
Sigma 160			.89				.54		.54	.73	.49										.82	
Xi 140		.69				.54	.54									.82						
Xi 150			.86				.54						.54					.79				
Xi 160				.86			.74			.27	.69		.27							.79		

Table 6. Overall Detection Efficiencies

	I. $N_o = 100$						II. $N_o = 70$
Momentum	π, K	$\bar{p}$	Σ	Ξ	Ω	$\bar{d}$	Ξ
140	.999	.97	.98	.97	.92	.86	.92
150	.98	.995	.97	.95	.95	.79	.87
160	.997	.993	.97	.975	.95	.83	.935

FIGURE CAPTIONS

Fig. 1. Proposed layout of the hyperon beam, showing the 5-meter magnetic channel, quadrupole pair, Cerenkov detector, and high-precision proportional counter planes for the accurate determination of the particle direction.

Fig. 2. Lateral distribution of beam emerging from quadrupole pair, vs. momentum. Within the 140-160 GeV/c acceptance band the full width is about 1.7 cm; but at any given momentum the particles are spread over about 0.7 cm.

Fig. 3. Horizontal angle vs. momentum within the momentum acceptance band. The overall angular spread is over 3 mrad, but the correlation of direction with momentum is excellent, the spread at any given momentum being about $\pm$ 0.1 mrad.

Fig. 4. Vertical position vs. momentum. There is essentially no correlation, the beam occupying about $\pm$ 1.5 cm.

Fig. 5. Vertical direction vs. momentum. The mean direction is independent of momentum, but the spread at any given momentum varies. It is a minimum at the "waist" at about 158 GeV/c, where it is only $\pm$ 0.04 mrad, but reaches about $\pm$ 0.1 mrad 10 GeV/c away. The vertical tuning needs to be changed to move the waist to 150 GeV/c. The extremely strict parallelism of the beam in the vertical direction means that the centers of all the Cerenkov rings will lie on a straight horizontal line.

Fig. 6. The Cerenkov circles for Ξ^-, Ω^-, and $\bar{d}$ at 140, 150 and 160 GeV/c, showing the approximate focusing for each kind of particle, the considerable overlapping at the right hand side, and the possibility of mass determination even without using the focus. Centers for each momentum are shown. n = 1.00011.

Fig. 7. Same as Fig. 6, but adding the other particles: Σ^-, $\bar{p}$, K^- and $(e\mu\pi)^-$.

Fig. 8. The use of concave mirror segments in the Cerenkov ring image plane to separate and collect the light falling on a specified symmetrical pair of segments.

a. A pair of circular segments in the image plane, seen from the direction of the incident light.

b. A slight tilt of the axis of the segmented mirror results in the collection of the light in a phototube out of the way of the incident light. Note that the focus of the incident Cerenkov light must be at the mirror plane in order to use the mirror segments as velocity slits.

Fig. 9. Plan of construction of the Cerenkov detector showing the 5-meter radiator length; the spherical mirror with a focal length of about 5.5 meters, whose image is reflected by the 45° plane mirror to the image plane mirror off to one side; the segmented image plane mirror array, composed of segments of mirrors whose focal length is about 60 cm; and the array of off-axis photomultipliers which collect the light from the segments.

Fig. 10. Projection in the Cerenkov ring image plane of an array of mirror segments adequate to separate and identify all the various incident particles. Note the bilateral symmetry about the horizontal momentum dispersion axis.

Fig. 11. Scale drawing of the layout of 1.5 inch photomultiplier tubes designed to receive the light from the mirror layout of Fig. 10. Each tube is labelled by the segment whose light it collects. The mirror layout is shown for comparison. The disposition depends upon the focal length of the image plane segments; it is given here for a 55-cm focal length.

Fig. 12. Matrix of logical coincidences needed in synthesizing a selection logic for the various particles. Each unambiguous logical intersection is labelled by the particle it represents. Some segments, numbered in parentheses, - e.g. those at the trajectory foci, always represent a unique particle and need not be in coincidence.

Fig. 13. Total number of photoelectrons in the image ring as a function of Cerenkov cone angle, for a 5-meter radiator of n = 1.00011. Two different photocathode efficiencies, corresponding to the values of N_o = 100 and 70, are plotted.

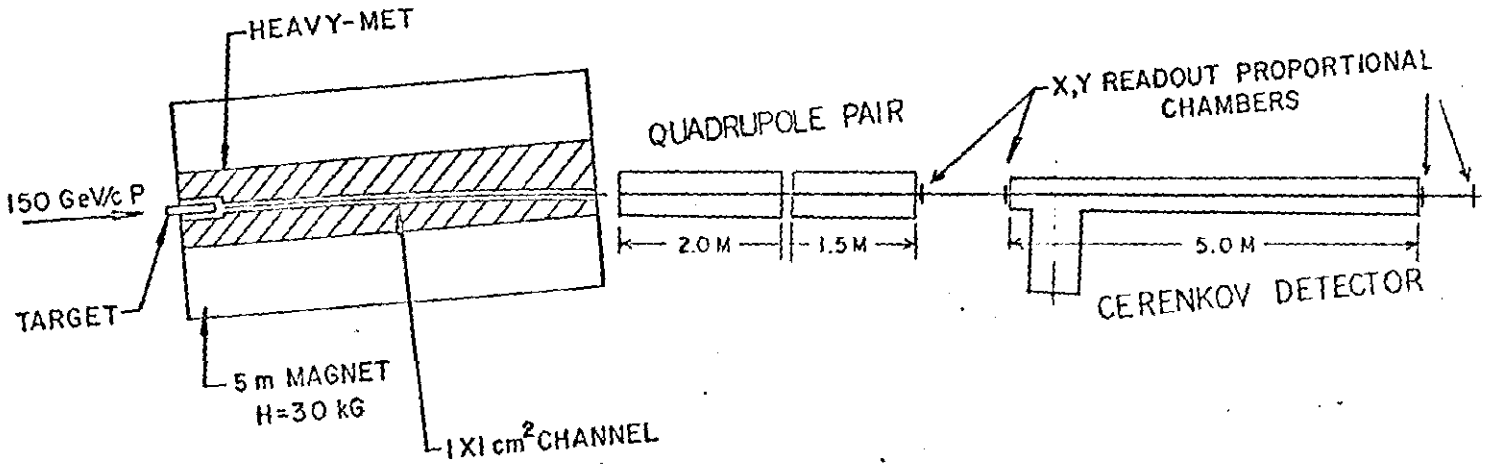

Fig. 1

FN-234
2526.000

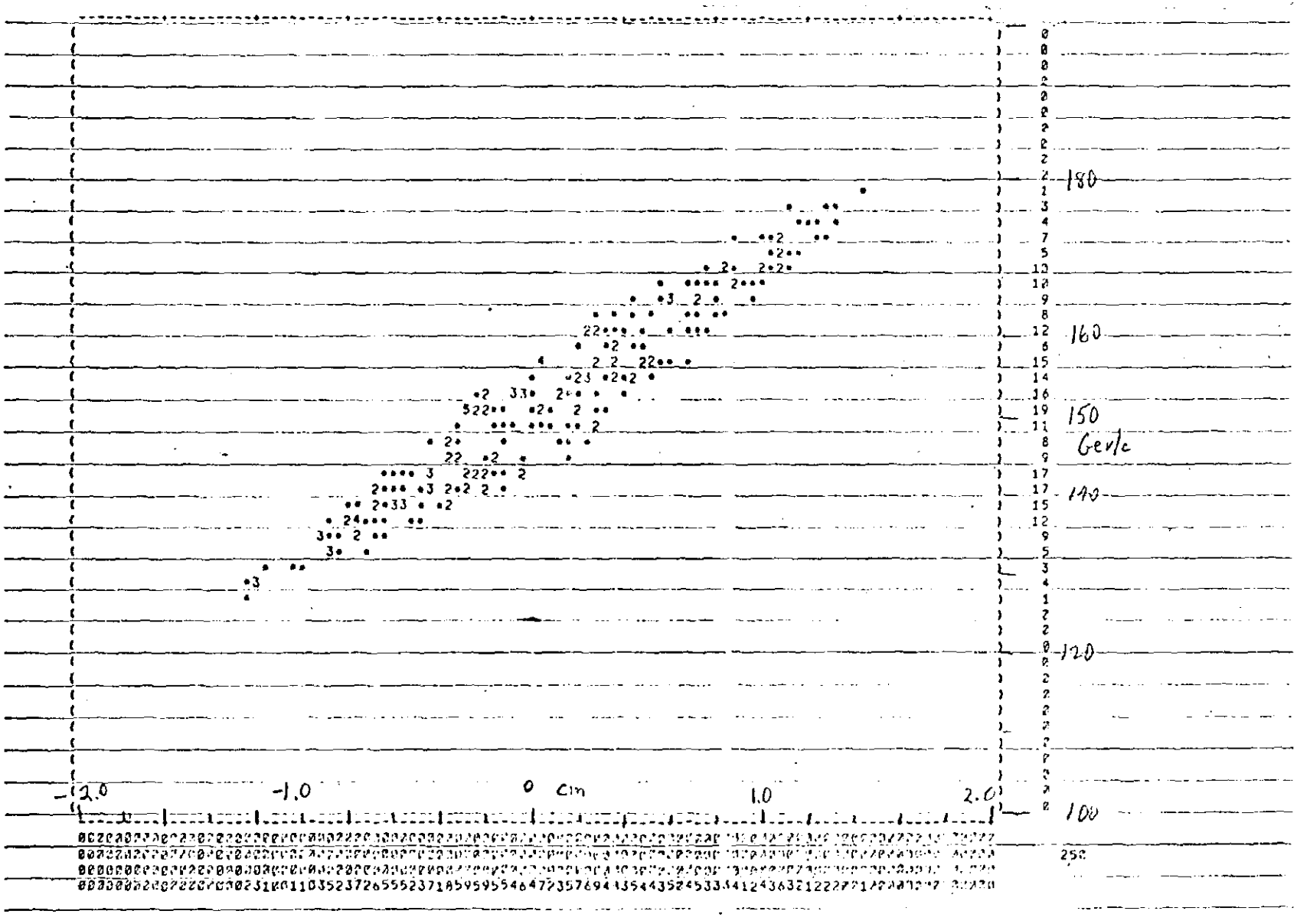

Fig. 2

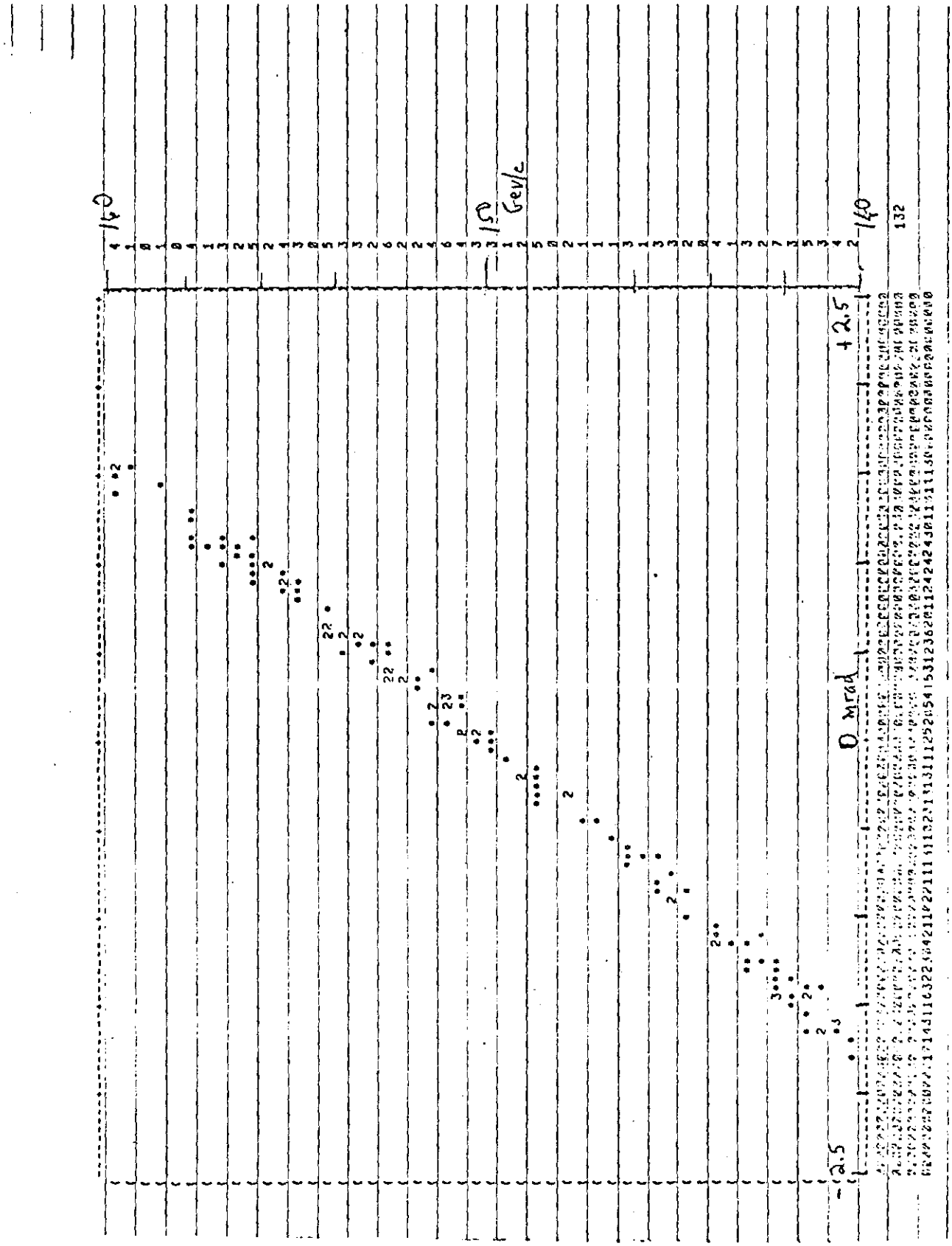

Fig. 3

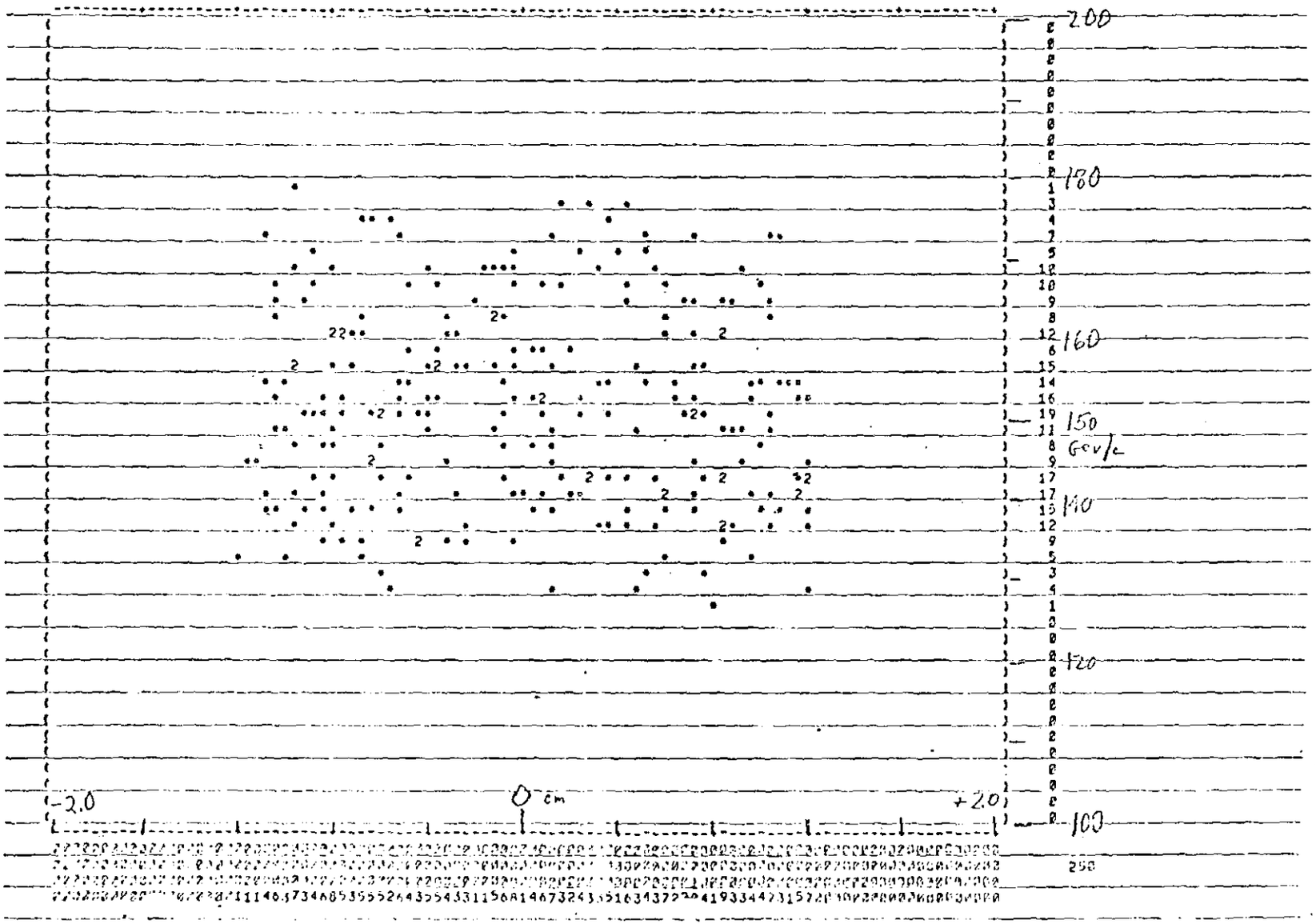

Fig. 4

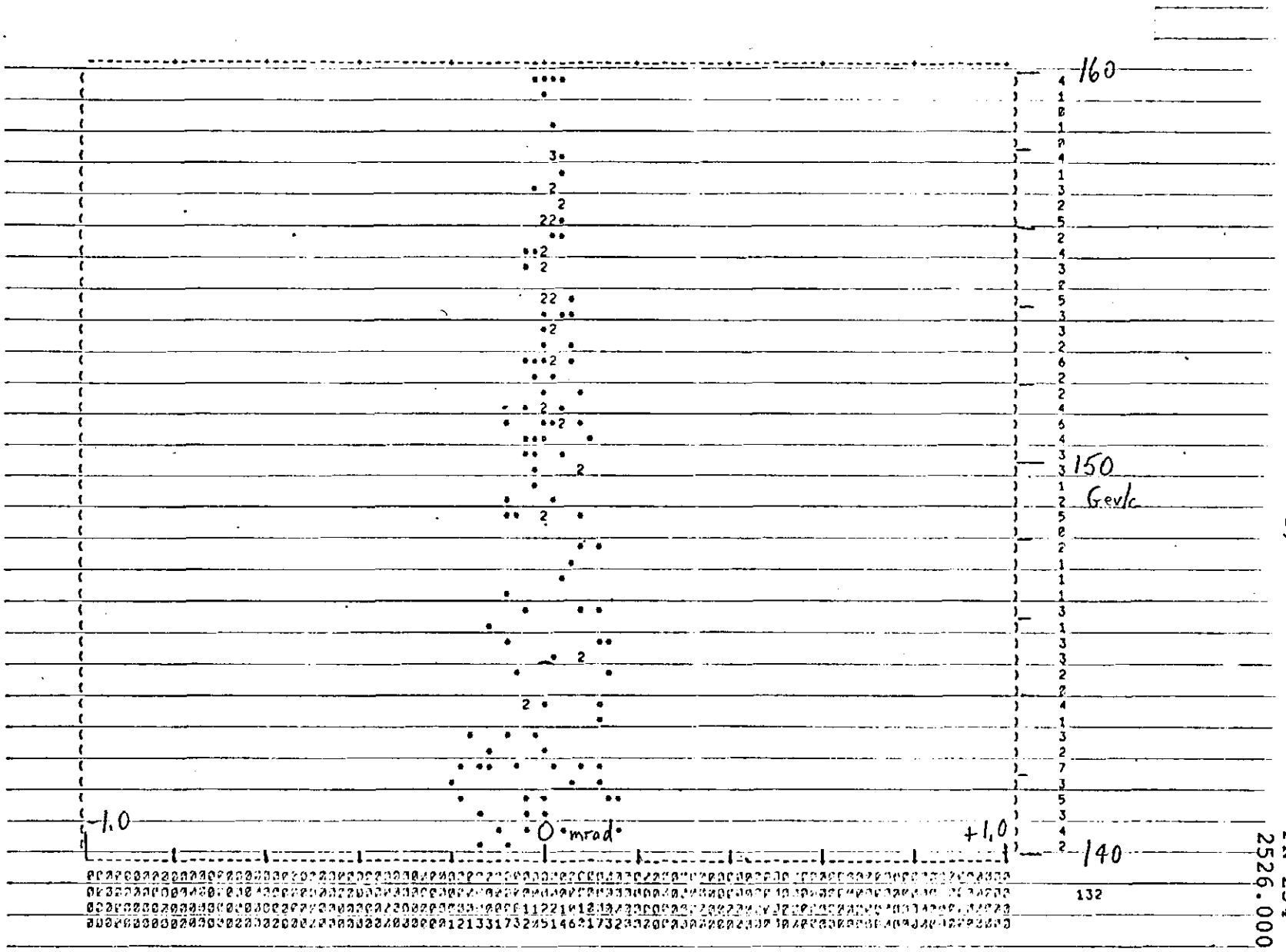

Fig. 5

FN-234
2526.000

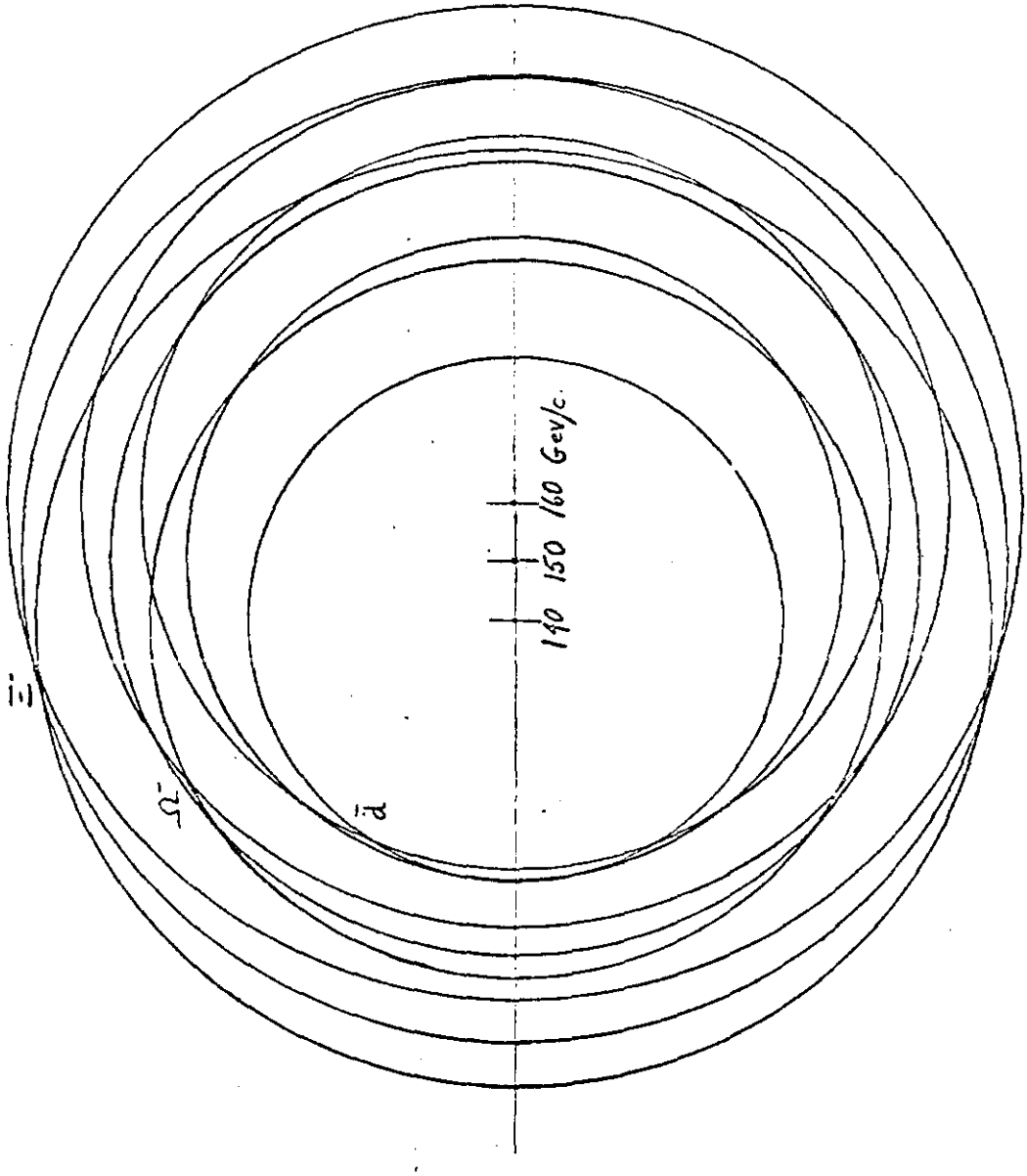

Fig.6

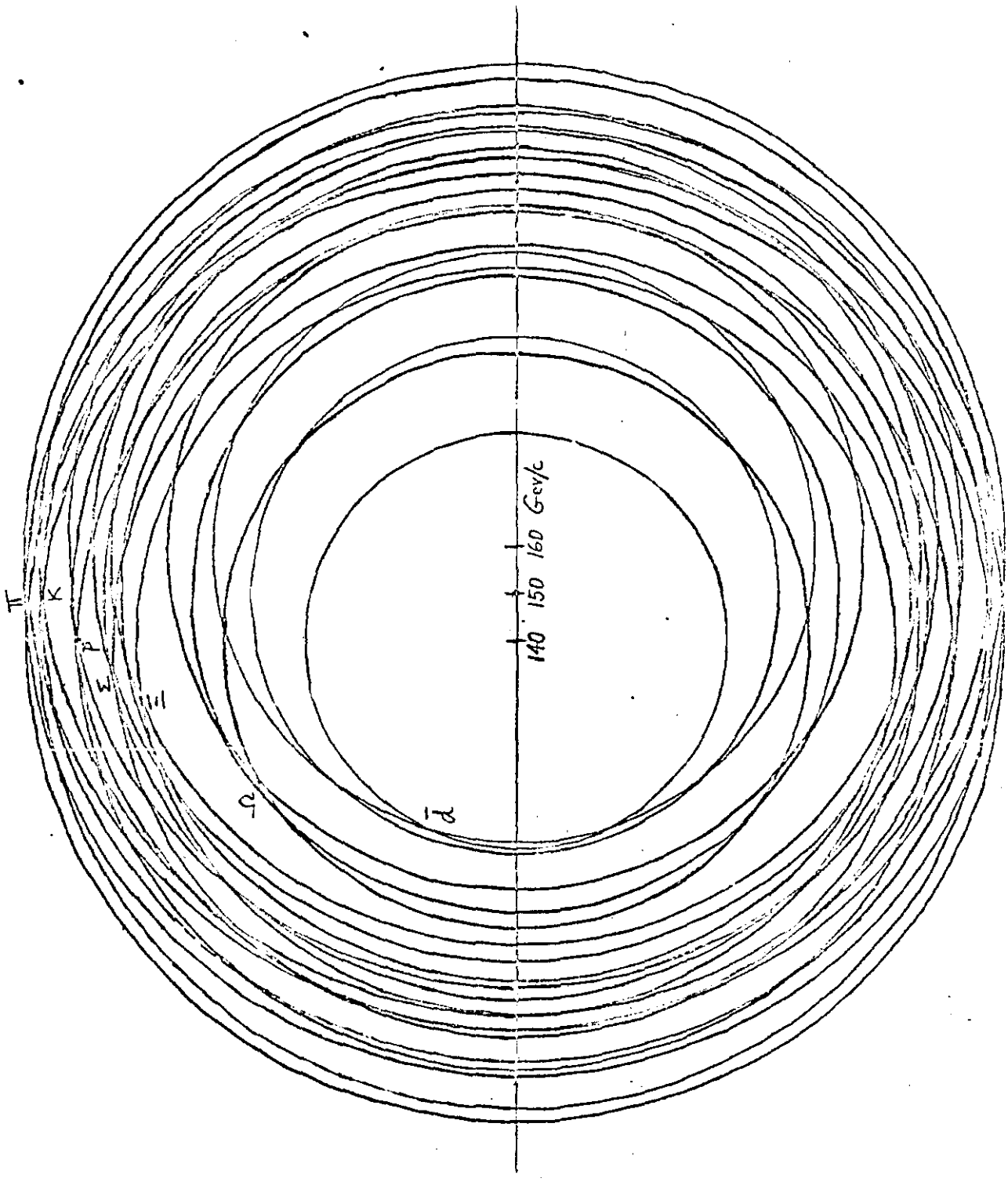

Fig. 7

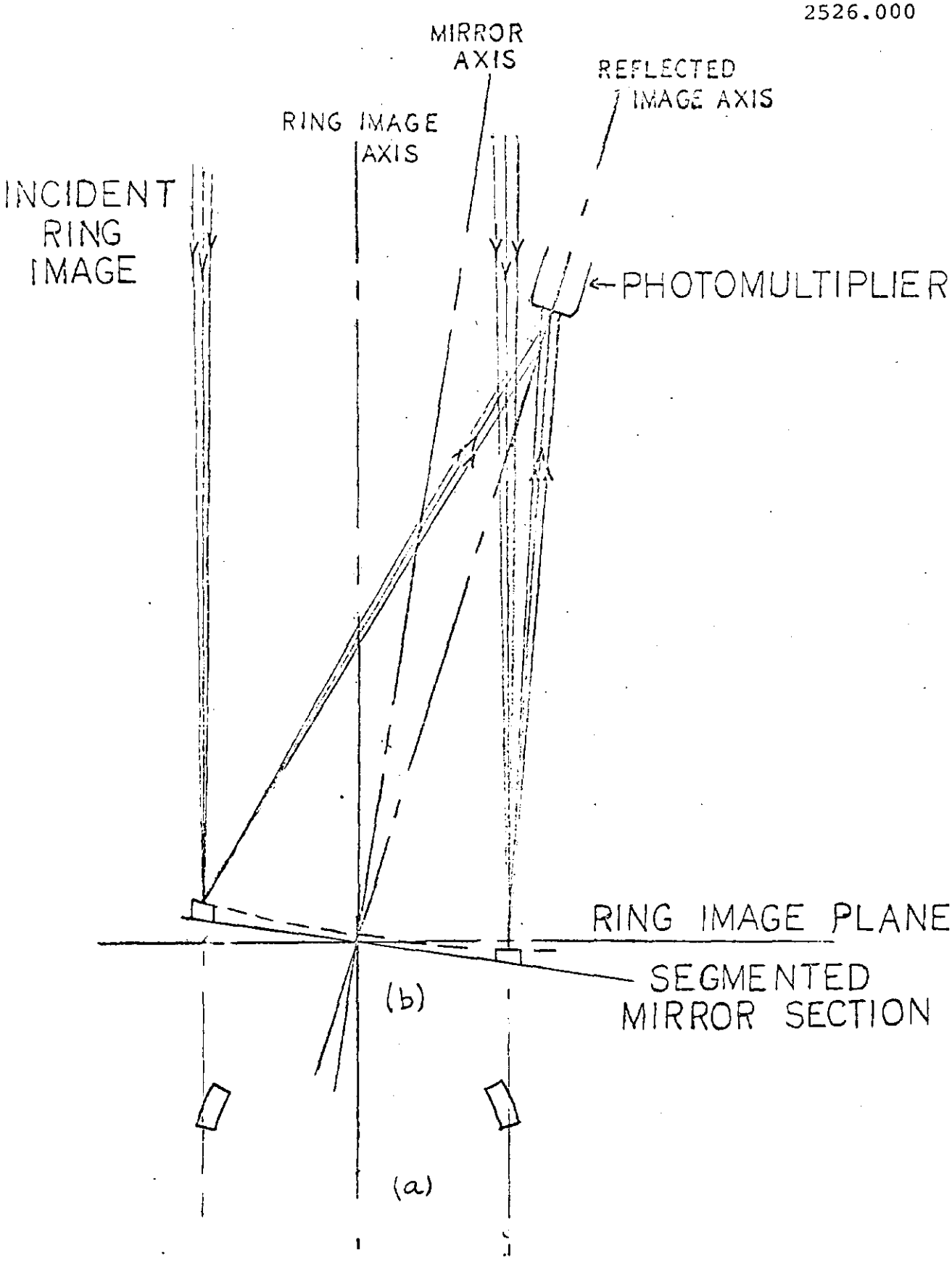
MIRROR AXIS
REFLECTED IMAGE AXIS
RING IMAGE AXIS
INCIDENT RING IMAGE
PHOTOMULTIPLIER
RING IMAGE PLANE
SEGMENTED MIRROR SECTION
(b)
(a)

Fig. 8

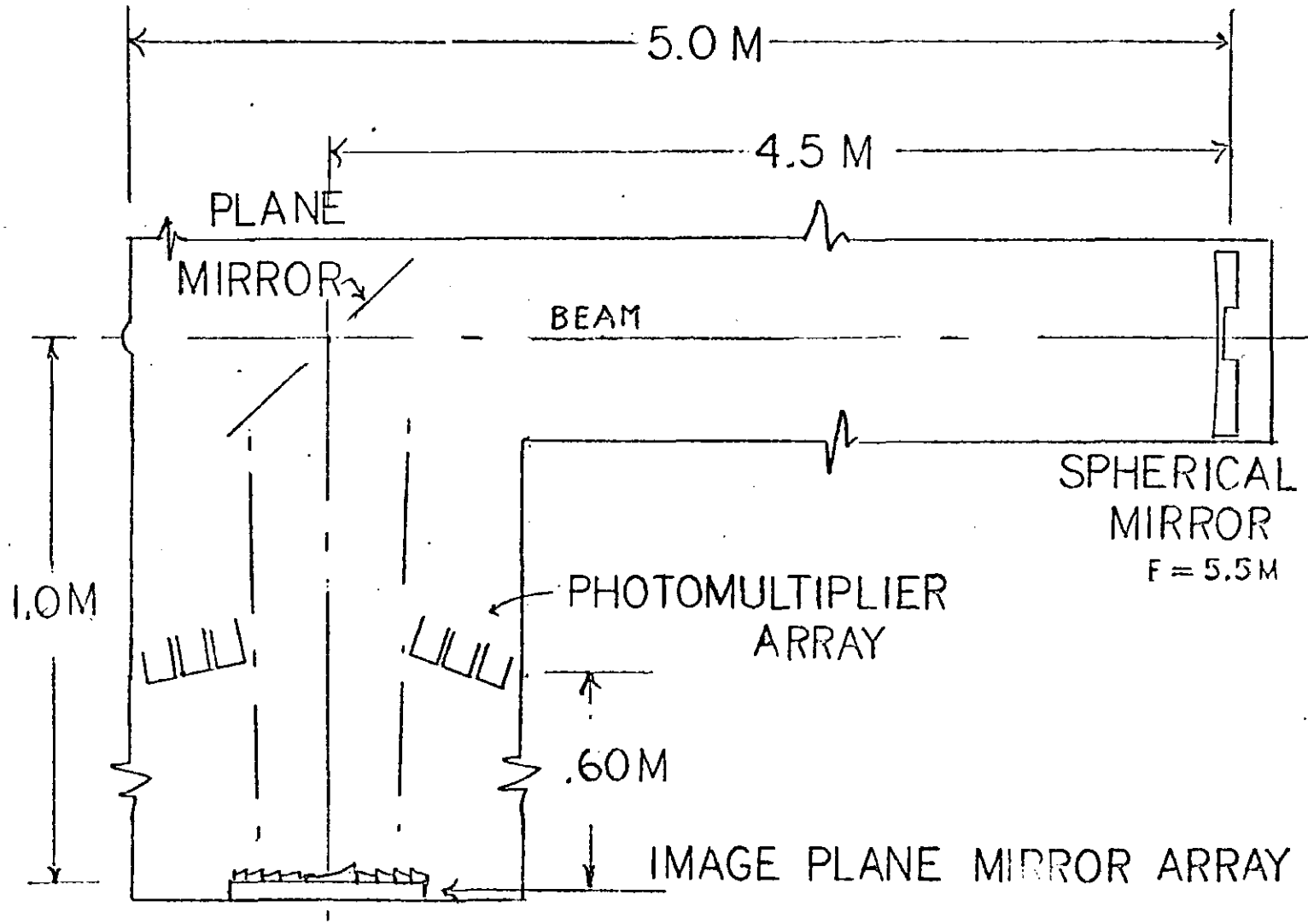

Fig. 9

FN-234
2526.000

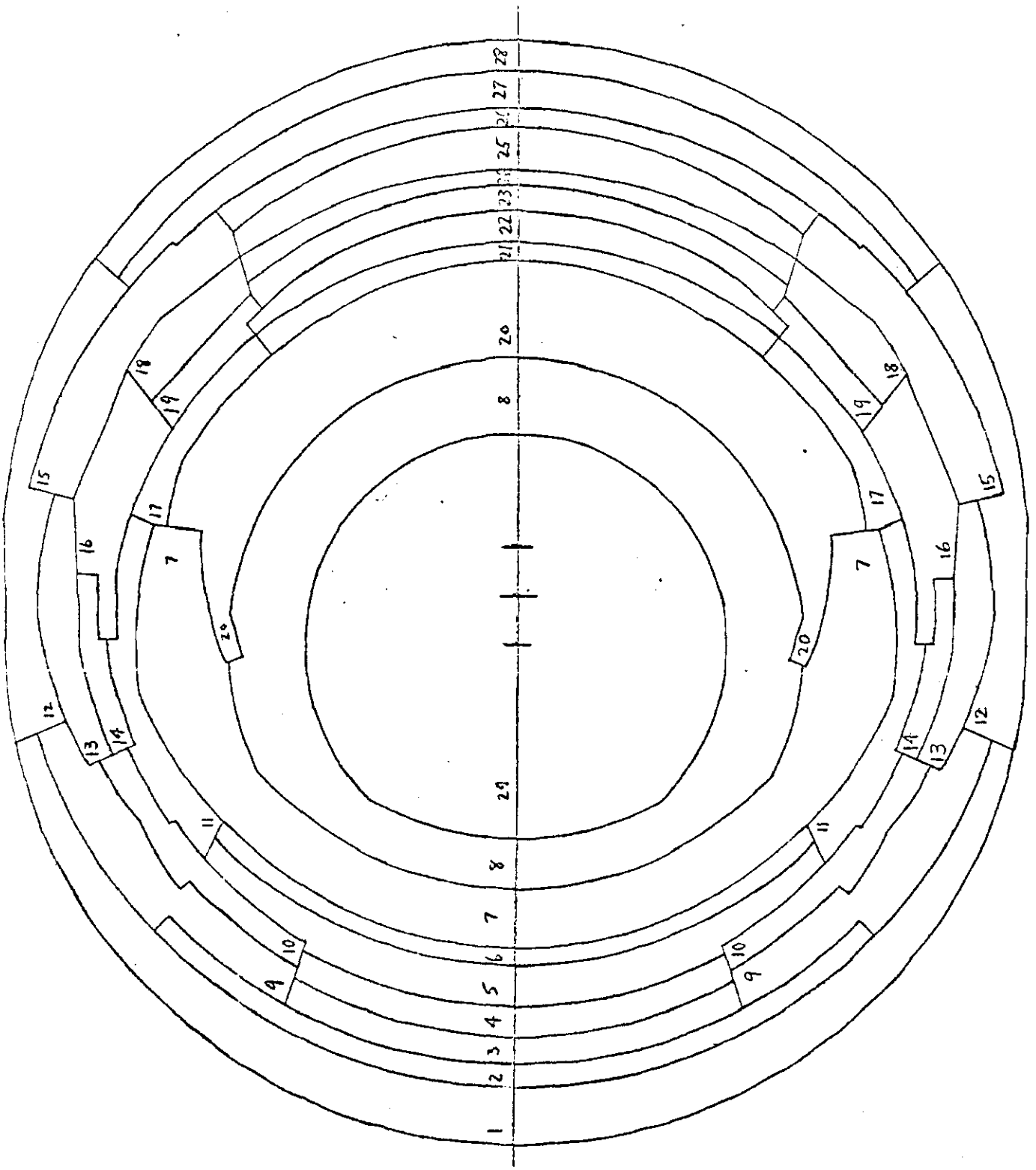
28
27
26
25
24
23
22
21
20
8
29
8
7
6
5
4
3
2
1
18
19
15
17
16
7
20
12
13
14
11
10
9

Fig 10

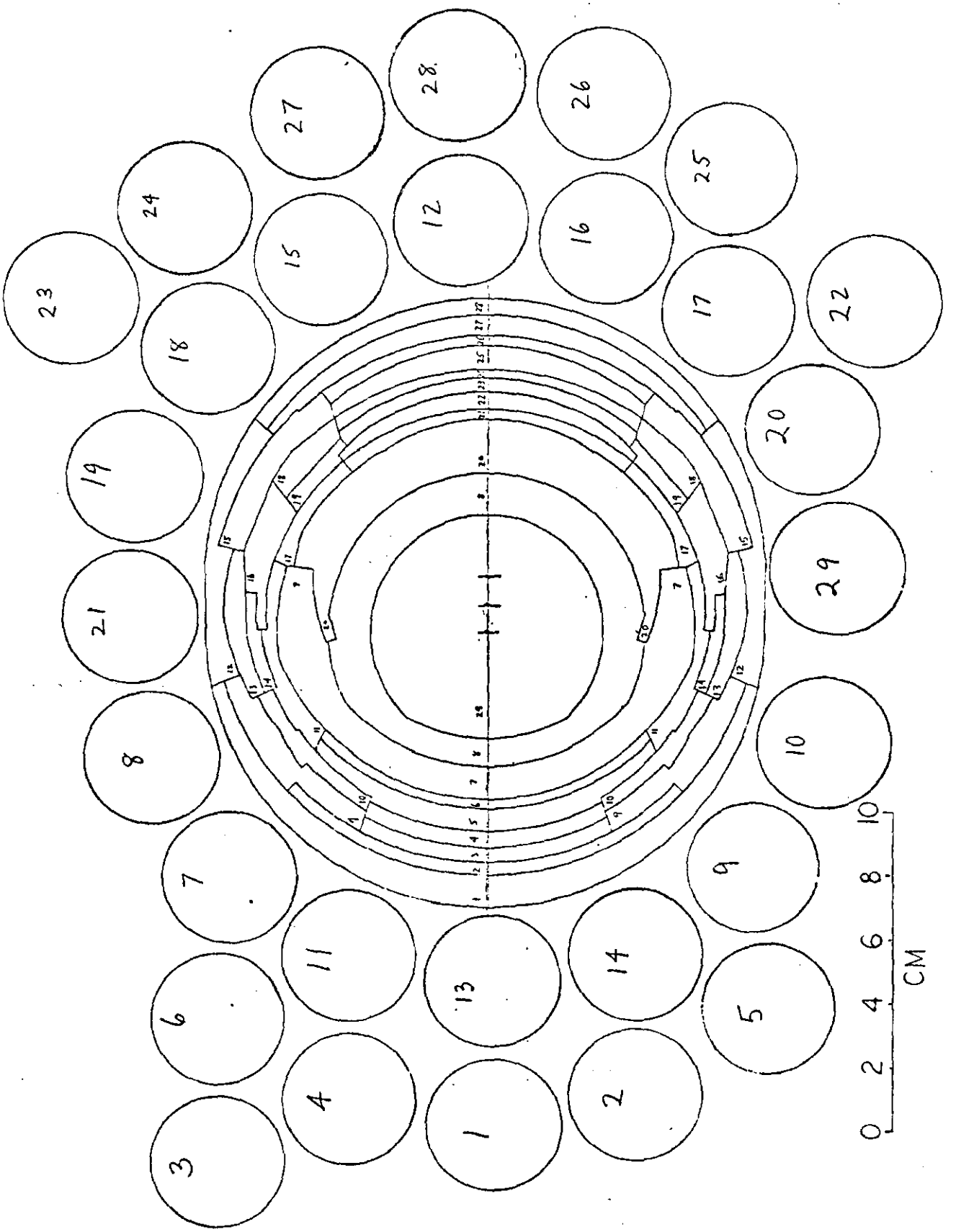
1
2
3
4
5
6
7
8
9
10
11
12
13
14
15
16
17
18
19
20
21
22
23
24
25
26
27
28
29
0 2 4 6 8 10
CM

Fig. 11

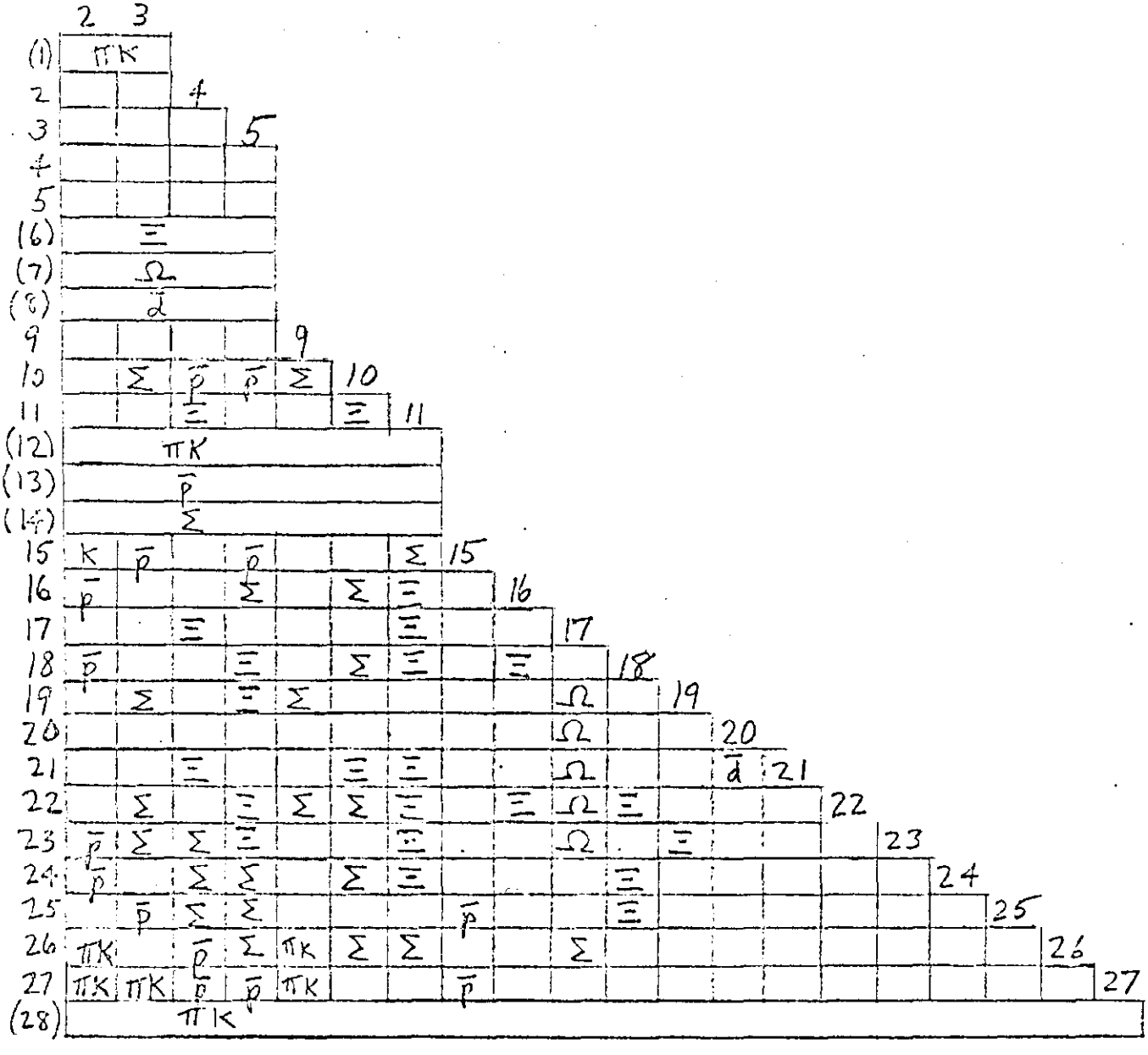

Fig. 12

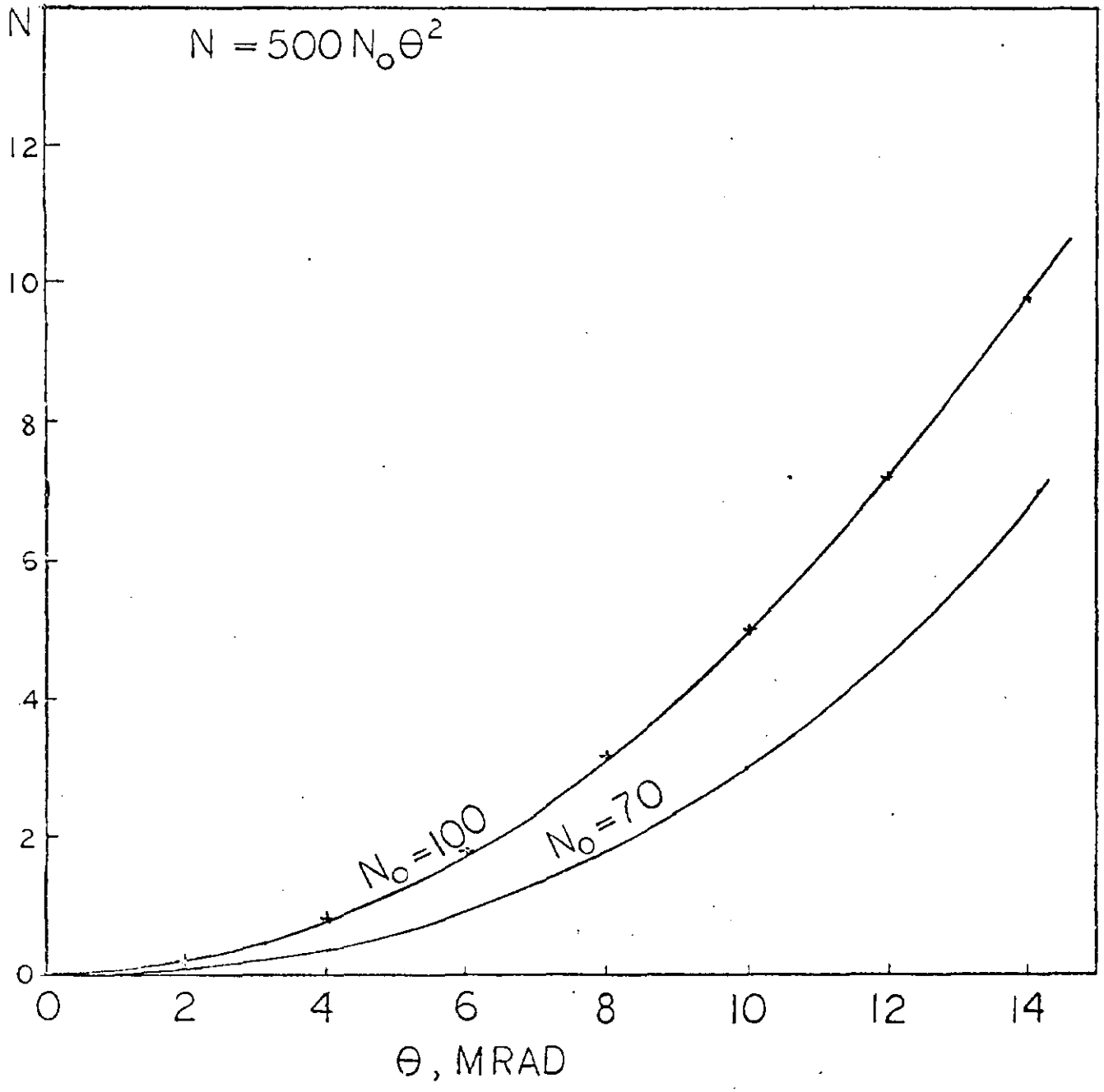

Fig. 13